Supporting Information

Measuring Residual Dipolar Couplings in Excited Conformational States of Nucleic Acids by CEST NMR Spectroscopy

Bo Zhao[†,‡] and Qi Zhang*[,†]

[†]Department of Biochemistry and Biophysics and [‡]Department of Chemistry, University of North Carolina at Chapel Hill, Chapel Hill, NC 27599, United States

Supporting Material and Methods

Sample preparation. Guanosine-specifically $^{13}C/^{15}N$-labeled *Bacillus cereus* fluoride riboswitch samples were prepared as described previously.[1] Briefly, after *in vitro* transcription and purification, the RNA samples were exchanged and concentrated to 1mM concentration in NMR buffer (10 mM sodium phosphate with pH 6.4, 50mM KCl, 50μM EDTA), which were subsequently lyophilized and re-dissolved in the same volume of 99.996% D_2O (Sigma).

NMR Spectroscopy and Data Analysis. All NMR experiments were carried out on a Bruker Avance III 600 spectrometer equipped with 5mm triple-resonance cryogenic probes at 303K. ^{13}C HSQC and TROSY/anti-TROSY selected CEST experiments are detailed below. One-bond ^{13}C-^{1}H RDCs were measured using 2D ^{1}H-^{13}C S^{3}CT-HSQC[2] in 9.7 mg/ml Pf1 phage alignment media (ASLA Biotech, Ltd) as described previously.[3] Errors in RDC measurements were calculated based on errors in ^{13}C-^{1}H splittings that were estimated based on measurements of splittings in ^{1}H and ^{13}C dimensions. All NMR spectra were processed and analyzed using NMRPipe/NMRDraw,[4] NMRView,[5] and Sparky 3.110. (University of California, San Francisco, CA).

2D ^{13}C HSQC CEST

2D ^{13}C HSQC CEST experiments were carried out using our previously developed nucleic-acid-optimized ^{13}C CEST pulse sequence[1] with and without a 3.5 kHz field $90_x240_y90_x$ composite pulse for ^{1}H decoupling during the CEST relaxation period (T_{EX}). For completeness, the ^{1}H-coupled ^{13}C HSQC CEST pulse sequence is included in Figure S1. A recycle delay of 1.5 s, T_{EX} = 0.3 s, and T_{MAX} = 0.305 s were used for all ^{13}C HSQC CEST measurements. Three spectra with T_{EX} = 0 s were recorded for reference in data fitting and error estimation.

For experiments on base carbon C8s, the ^{13}C carrier was set to 135.75 ppm with a spectral width of 6.5 ppm. Selective pulses *a*, *b*, and *c* were 750 μs Q3 (on-resonance), 1000 μs reburp (on-resonance), 500 μs isnob2 (-5.89 kHz off-resonance), respectively. Two ^{13}C B_1 fields were used: $\omega/2\pi$ = 16.44 Hz with a ^{13}C offset ranging from -990 to 990 Hz and a spacing of 30 Hz; $\omega/2\pi$ = 26.04 with a ^{13}C offset ranging between -1000 to 1000 Hz with a spacing of 40. For experiments on sugar carbon C1's, the ^{13}C carrier was set to 88.75 ppm with a spectral width of 4.2 ppm. Selective pulses *a*, *b*, and *c* were 1250 μs Q3 (0.6 kHz off-resonance), 1000 μs reburp (1.5 kHz off-resonance), 600 μs iburp2 (-5.76 kHz off-resonance), respectively. Two ^{13}C B_1 fields were used: $\omega/2\pi$ = 16.44 Hz with a ^{13}C offset ranging from -720 to 720 Hz and a spacing of 30 Hz; $\omega/2\pi$ = 26.04 with a ^{13}C offset ranging between -720 to 720 Hz with a spacing of 40 Hz. These spin-lock powers were calibrated according to the 1D approach by Guenneugues et al.[6] as previously described.[1] A total of 864 2D data were recorded for ^{1}H-decoupled and ^{1}H-coupled HSQC CEST measurements in the absence and presence of 9.7 mg/ml Pf1 phage alignment media.

2D ^{13}C TROSY/anti-TROSY selected CEST

The pulse sequences for 2D ^{13}C TROSY[7] selected (TS) and anti-TROSY selected (aTS) CEST experiments are shown in Figure S4, and employ various schemes developed in TS

$R_{1\rho}$ RD,[8] CPMG RD RDC,[9] ^{15}N TROSY CEST,[10] and nucleic-acid-optimized TROSY-detected (TD) $R_{1\rho}$ spin relaxation[11] experiments. The ^{15}N TROSY CEST experiment was developed for determining ES hydrogen exchange rates in excited states of proteins,[10] except the S^{3}CT (spin-state-selective coherence transfer) selective inversion pulse was exempt during the CEST relaxation period (T_{EX}). Here, the TROSY or the anti-TROSY ^{13}C magnetization is first selected via a S^{3}E (spin-state-selective excitation) filter[12] prior to T_{EX}. During T_{EX}, a S^{3}CT selective-inversion element[13] is employed to suppress cross-relaxation between the TROSY and the anti-TROSY components. During the subsequent chemical shift coding and detection period, the TROSY components are maintained throughout the experiment for TS CEST pulse sequence. For aTS CEST pulse sequence, the anti-TROSY components are converted to TROSY components after T_{EX} via a ^{1}H 180^o pulse, a scheme that was previously employed in the CPMG-RD based RDC measurements.[9] By this conversion, the aTS experiment delivers apparent TROSY spectra with better resolution and enhanced detection, but reports exchanges between anti-TROSY components of ground and excited states, where the resulting CEST profiles display positions of intensity dips that match corresponding anti-TROSY chemical shifts. Given different relaxation properties of TROSY and anti-TROSY ^{13}C magnetizations, T_{EX} delays were optimized for each experiment as described below. To ensure uniform heating, a recycle delay of 1.5 s and T_{MAX} = 0.305 s were used for all ^{13}C TS/aTS CEST measurements. Three spectra with T_{EX} = 0 s were recorded for reference in data fitting and error estimation.

For experiments on base carbon C8s, the ^{13}C carrier was set to 136.45 ppm with a spectral width of 6.5 ppm. Selective pulses *a*, *b*, *c,* and *d* were 750 μs Q3 (on-resonance), 470 μs reburp (on-resonance), 500 μs isnob2 (-5.89 kHz off-resonance), a 1000 μs reburp (on-resonance), respectively. Two ^{13}C B_1 fields were used: for $\omega/2\pi$ = 16.04 Hz, the ^{13}C offset ranged between -1080 to 900 Hz with a spacing of 30 Hz; for $\omega/2\pi$ = 26.04, the ^{13}C

offset ranged between -1080 to 920 Hz with a spacing of 40. Because of the different relaxation behavior of the TROSY and anti-TROSY components, T_{EX} delays of 0.3s and 0.16s were used for TS and aTS experiments, respectively. For experiments on sugar carbon C1's, the ^{13}C carrier was set to 89.3 ppm with a spectral width of 4.2 ppm. Selective pulses *a*, *b*, *c,* and *d* were 1250 μs Q3 (0.6 kHz off-resonance), 780 μs reburp (2.1 kHz off-resonance), 600 μs iburp2 (-5.76 kHz off-resonance), and a 1000 μs repurb (1.5 kHz off-resonance), respectively. Two ^{13}C B_1 fields were used: $\omega/2\pi$ = 16.44 Hz with a ^{13}C offset ranging between -810 to 630 Hz with a spacing of 30 Hz; $\omega/2\pi$ = 26.04 with a ^{13}C offset ranging from -800 to 640 Hz with a spacing of 40 Hz. T_{EX} delays of 0.25s and 0.2s were used for TS and aTS experiments, respectively. A total of 864 2D data were recorded for TS and aTS CEST measurements in the absence and presence of 9.7 mg/ml Pf1 phage alignment media.

CEST Data Analysis

All CEST profiles (HSQC and TS/aTS) were obtained by normalizing the peak intensity as a function of spin-lock offset Ω, where $\Omega = \omega_{rf} - \Omega_{obs}$ is the frequency difference between the spin-lock carrier (ω_{rf}) and the observed peak (Ω_{obs}), to the peak intensity recorded at T_{EX} = 0 s. Errors in CEST measurements were estimated based on triplicate data points at T_{EX} = 0 and standard deviations in baselines of CEST profiles. The profiles of residues displaying conformational exchange were fit to a two-state exchange between ground state (*G*) and excited state (*E*) based on the Bloch-McConnell equation[14] that describes magnetization evolution in a coupled two-spin ^{13}C-^{1}H system.[15,16] For residues without conformational exchange, the two-state exchange model was simplified to a one-state model by fixing all exchange parameters (rate of exchange k_{ex} and excited-state population p_{ES}) to 0. For individual state (*i*), the evolution of its magnetization ($\mathbf{v}^i$) as a coupled two-spin ^{13}C-^{1}H system is described by,[15]

$$\frac{d}{dt}\mathbf{v}^i = -\mathbf{R}^i\mathbf{v}^i = \begin{pmatrix} R_2^i & \omega_C^i & 0 & \eta_{xy}^i & \pi J_{CH}^i & 0 \\ -\omega_C^i & R_2^i & \omega_1 & -\pi J_{CH}^i & \eta_{xy}^i & 0 \\ 0 & -\omega_1 & R_1^i & 0 & 0 & \eta_z^i \\ \eta_{xy}^i & \pi J_{CH}^i & 0 & R_{2HC}^i & \omega_C^i & 0 \\ -\pi J_{CH}^i & \eta_{xy}^i & 0 & -\omega_C^i & R_{2HC}^i & \omega_1 \\ 0 & 0 & \eta_z^i & 0 & -\omega_1 & R_{1HC}^i \end{pmatrix} \begin{pmatrix} C_x^i \\ C_y^i \\ C_z^i \\ 2H_zC_x^i \\ 2H_zC_y^i \\ 2H_zC_z^i \end{pmatrix}$$

where $R_1{}^i$ is the ^{13}C longitudinal relaxation rate, $R_2{}^i$ is the ^{13}C transverse relaxation, $R_{1HC}{}^i$ is the ^{13}C-^{1}H two-spin order relaxation rate, $R_{2HC}{}^i$ is the ^{13}C antiphase relaxation rate, $\eta_z{}^i$ is the C-H dipolar-dipolar/carbon CSA cross-correlated relaxation between the ^{13}C longitudinal and two-spin order elements, $\eta_{xy}{}^i$ is C-H dipolar-dipolar/carbon CSA cross-correlated relaxation between ^{13}C transverse and antiphase magnetizations, $\omega_C{}^i$ is the offset of the applied ^{13}C B_1 field (strength of ω_1) from state i (here ω^{GS} is obtained from the observed ground-state peak position and $\omega^{ES} = \omega^{GS} + \Delta\omega$, where $\Delta\omega$ is the chemical shift difference between the ground and excited states), and $J_{CH}{}^i$ is the ^{13}C-^{1}H splitting that corresponds to ^{13}C-^{1}H scalar coupling in isotropic solution and the sum of ^{13}C-^{1}H scalar coupling and residual dipolar coupling in the presence of alignment media. For TS/aTS experiments, since the observed ground-state peak has the chemical shift of the TROSY ^{13}C magnetization, the ω^{GS} is input as $\omega_{obs}{}^{GS} - J^{GS}{}_{CH}/2$. In addition, for joint analysis of HSQC CEST profiles measured in the absence and presence of ^{1}H decoupling, all two-spin relaxation parameters ($R_{1HC}{}^i$, $R_{2HC}{}^i$, $\eta_z{}^i$, $\eta_{xy}{}^i$, and $J_{CH}{}^i$) were set to 0 for the ^{1}H-decoupled CEST profiles. For a two-state exchange model, the evolution of magnetizations of ground and excited states is described by,

$$\frac{d}{dt}\boldsymbol{\sigma}(t) = -\mathbf{L}\cdot\begin{bmatrix} \mathbf{v}^{GS} \\ \mathbf{v}^{ES} \end{bmatrix} = \left(\begin{bmatrix} \mathbf{R}^{GS} & \mathbf{0}_6 \\ \mathbf{0}_6 & \mathbf{R}^{ES} \end{bmatrix} + \begin{bmatrix} -k_{GE} & k_{EG} \\ k_{GE} & -k_{EG} \end{bmatrix} \otimes \mathbf{1}_6 \right) \cdot \begin{bmatrix} \mathbf{v}^{GS} \\ \mathbf{v}^{ES} \end{bmatrix}$$

where $\mathbf{v}^{GS/ES}$ and $\mathbf{R}^{GS/ES}$ are magnetization and relaxation matrices for ground and excited states as detailed above, $\mathbf{0}_6$ and $\mathbf{1}_6$ are 6x6 null and identity matrices, and k_{GE} and k_{EG} are

forward and backward exchange rates, which are defined as $k_{GE} = p_E\, k_{ex}$ and $k_{EG} = p_G\, k_{ex}$. Here, $k_{ex} = k_{GE} + k_{EG}$ is the rate of exchange, and p_G and p_E are populations of ground and excited states, respectively. Magnetizations at the beginning of the T_{EX} period are along Z and are assumed to be in equilibrium between ground and excited states (neglecting relaxation differences during INEPT transfer). Hence, the initial magnetization conditions at $T_{EX} = 0$ for ground and excite states are set to be their corresponding populations as p_G and p_E. For HSQC CEST, the initial magnetizations are pure ^{13}C magnetization, and for TS/aTS CEST experiments, the initial magnetizations are TROSY/anti-TROSY ^{13}C magnetization components. In addition, for TS/aTS CEST experiments, ^{13}C magnetizations were first simulated for $T_{EX}/2$, then selectively inverted by the S^3CT element, and subsequently simulated for a second $T_{EX}/2$. For residues from the stable P2 stem, a simple one-state model is employed in fitting their individual set of CEST profiles, whose fitting parameters are R_1^G, R_2^G, η_z^G, η_{xy}^G, R_{1HC}^G, R_{2HC}^G, and J_{CH}^G. For G8 and G10, since they have been previously shown in undergoing a global exchange process, all their CEST profiles are fit with global exchange parameters (k_{ex} and p_E) and individual relaxation rates, chemical shift differences and ^{13}C-^1H splittings ($R_1^{G/E}$, $R_2^{G/E}$, $\eta_z^{G/E}$, $\eta_{xy}^{G/E}$, $R_{1HC}^{G/E}$, $R_{2HC}^{G/E}$, $\Delta\omega$, and $J_{CH}^{G/E}$). During the analysis, we assumed that $R_1^G = R_1^E$, $\eta_z^G = \eta_z^E$, and $R_{1HC}^G = R_{1HC}^E$, as the data does not constrain determination of these longitudinal relaxation parameters. While different R_2^G and R_2^E are essential for accurate data analysis as described previously,[1] we found that different $\eta_{xy}^{G/E}$ values are not required, as including different values does not improve overall fitting quality. In addition, we employed a previously reported relationship between relaxation rates ($R_{2HC}^{G/E} = R_2^{G/E} + R_{1HC} - R_1$) to further simply data analysis.[17] In summary, for a spin that undergoes a two-state exchange model, there are a total of 11 fitting parameters, 2 of which are global parameters and 9 of which are spin-specific parameters. As described previously,[1] for C1' CEST profiles (HSQC and TS/aTS), C1'-C2' scalar couplings with an averaged value of 45 Hz measured from a non-decoupled HSQC experiment were

implemented to calculate two CEST profiles, one representative of C2' in the 'down' state and another in the 'up' state.[18] The two CEST profiles were then averaged in the resulting fit to obtain the observed CEST profile. The profiles were fit using an in-house MATLAB® program with a Levenberg-Marquardt algorithm and chi-square values $\chi^2 = \sum^{N}\left(\left(I_i^{\exp} - I_i^{calc}\right)/\sigma_i^{\exp}\right)^2$ were calculated. Fitting errors were estimated from both the Jacobian output and from 200 Monte-Carlo simulations[19], and the larger errors from these two methods were reported.

Table S1. Directly measured ^{13}C-^{1}H splittings and RDCs for the ground state of G-labeled ligand-free fluoride riboswitch in the absence and presence of 9.7 mg/ml Pf1 phage using conventional ^{13}C-^{1}H S^3CT-HSQC experiments.

Residue		Direct Measurement		
		J_{CH} *(Hz)*	$J_{CH}+D_{CH}$ *(Hz)*	D_{CH} *(Hz)*
$G08_{GS}$	C8H8	214.7 ± 1.5	220.5 ± 1.5	5.8 ± 2.1
	C1'H1'	164.8 ± 1.5	172.7 ± 1.5	7.9 ± 2.1
$G10_{GS}$	C8H8	214.8 ± 1.5	220.6 ± 1.5	5.8 ± 2.1
	C1'H1'	166.5 ± 1.5	167.9 ± 1.5	1.4 ± 2.1
$G23_{GS}$	C8H8	218.1 ± 1.5	212.8 ± 1.5	-5.3 ± 2.1
	C1'H1'	176.6 ± 1.5	168.8 ± 1.5	-7.8 ± 2.1
$G30_{GS}$	C8H8	214.5 ± 1.5	220.1 ± 1.5	5.6 ± 2.1
	C1'H1'	166.7 ± 1.5	170.0 ± 1.5	3.3 ± 2.1
$G31_{GS}$	C8H8	216.8 ± 1.5	222.9 ± 1.5	6.1 ± 2.1
	C1'H1'	173.7 ± 1.5	168.3 ± 1.5	-5.4 ± 2.1
$G33_{GS}$	C8H8	214.3 ± 1.5	224.2 ± 1.5	9.9 ± 2.1
	C1'H1'	175.7 ± 1.5	176.1 ± 1.5	0.4 ± 2.1

Table S2: Extracted ^{13}C-^{1}H splittings and RDCs for the ground and excited states of G-labeled ligand-free fluoride riboswitch in the absence and presence of 9.7 mg/ml Pf1 phage using 2D ^{13}C HSQC CEST experiments.

Residue		HSQC CEST Measurement		
		J_{CH} (Hz)	$J_{CH}+D_{CH}$ (Hz)	D_{CH} (Hz)
$G08_{GS}$	C8H8	213.8 ± 1.2	222.8 ± 1.2	9.0 ± 1.6
	C1'H1'	164.0 ± 1.4	172.8 ± 1.6	8.8 ± 2.1
$G10_{GS}$	C8H8	215.2 ± 1.4	221.2 ± 1.1	6.0 ± 1.8
	C1'H1'	167.5 ± 1.6	168.8 ± 1.6	1.3 ± 2.3
$G23_{GS}$	C8H8	213.9 ± 1.6	209.5 ± 1.8	-4.4 ± 2.3
	C1'H1'	174.8 ± 2.0	163.0 ± 1.9	-11.8 ± 2.7
$G30_{GS}$	C8H8	215.5 ± 0.7	218.1 ± 1.1	2.6 ± 1.3
	C1'H1'	165.9 ± 1.3	169.5 ± 1.3	3.6 ± 1.8
$G31_{GS}$	C8H8	217.1 ± 0.8	223.2 ± 0.9	6.1 ± 1.2
	C1'H1'	173.0 ± 3.2	167.1 ± 1.7	-5.9 ± 3.6
$G33_{GS}$	C8H8	214.1 ± 0.9	221.0 ± 1.2	6.9 ± 1.5
	C1'H1'	175.7 ± 1.4	177.2 ± 1.3	1.5 ± 1.9
$G08_{ES}$	C8H8	218.9 ± 2.5	207.7 ± 2.6	-11.2 ± 3.6
	C1'H1'	175.0 ± 2.5	152.5 ± 2.6	-22.5 ± 3.6
$G10_{ES}$	C8H8	214.3 ± 2.9	233.8 ± 2.9	19.5 ± 4.1
	C1'H1'	174.5 ± 3.1	160.9 ± 3.2	-13.6 ± 4.4

Table S3. Extracted global exchange parameters and chemical shift differences between ground and excited states of G8 and G10 in the absence and presence of 9.7 mg/ml Pf1 phage using 2D ^{13}C HSQC CEST experiments.

Residue	Isotropic			Pf1 Phage		
	k_{ex} (s^{-1})	p_{ES} (%)	$\Delta\varpi_{GE}$(ppm)	k_{ex} (s^{-1})	p_{ES} (%)	$\Delta\varpi_{GE}$(ppm)
G08 C8	108 ± 5	9.4 ± 0.1	-4.12 ± 0.01	88 ± 5	10.1 ± 0.2	-4.07 ± 0.01
G08 C1'			3.39 ± 0.01			3.39 ± 0.01
G10 C8			-3.98 ± 0.01			-4.00 ± 0.01
G10 C1'			2.39 ± 0.01			2.39 ± 0.01

Table S4: Extracted ^{13}C-^{1}H splittings and RDCs for the ground and excited states of G-labeled ligand-free fluoride riboswitch in the absence and presence of 9.7 mg/ml Pf1 phage using 2D ^{13}C TROSY/anti-TROSY selected CEST experiments.

Residue		TS/aTS CEST Measurement		
		J_{CH} (Hz)	$J_{CH}+D_{CH}$ (Hz)	D_{CH} (Hz)
$G08_{GS}$	C8H8	215.0 ± 0.9	222.5 ± 1.0	7.5 ± 1.3
	C1'H1'	160.1 ± 1.0	169.2 ± 1.2	9.1 ± 1.5
$G10_{GS}$	C8H8	215.2 ± 0.7	218.0 ± 0.8	2.8 ± 1.0
	C1'H1'	163.9 ± 1.0	165.5 ± 1.1	1.6 ± 1.5
$G23_{GS}$	C8H8	221.8 ± 1.4	217.8 ± 1.2	-4.0 ± 1.9
	C1'H1'	172.6 ± 1.6	164.0 ± 4.0	-8.6 ± 4.3
$G30_{GS}$	C8H8	213.1 ± 1.1	217.3 ± 1.2	4.2 ± 1.6
	C1'H1'	167.1 ± 1.6	172.8 ± 1.8	5.7 ± 2.4
$G31_{GS}$	C8H8	217.7 ± 0.7	222.3 ± 0.7	4.6 ± 1.0
	C1'H1'	173.6 ± 1.6	166.1 ± 1.8	-7.5 ± 2.4
$G33_{GS}$	C8H8	214.9 ± 1.0	223.2 ± 0.9	8.3 ± 1.4
	C1'H1'	171.8 ± 1.3	175.0 ± 2.5	3.2 ± 2.8
$G08_{ES}$	C8H8	215.8 ± 2.8	211.1 ± 3.1	-4.7 ± 4.1
	C1'H1'	175.2 ± 2.6	154.4 ± 3.2	-20.8 ± 4.1
$G10_{ES}$	C8H8	211.0 ± 2.8	234.8 ± 3.2	23.8 ± 4.2
	C1'H1'	170.2 ± 3.0	155.0 ± 3.5	-15.2 ± 4.6

Table S5. Extracted global exchange parameters and chemical shift differences between ground and excited states of G8 and G10 in the absence and presence of 9.7 mg/ml Pf1 phage using 2D ^{13}C TROSY/anti-TROSY selected CEST experiments.

Residue	Isotropic			Pf1 Phage		
	k_{ex} (s^{-1})	p_{ES} (%)	$\Delta\varpi_{GE}$(ppm)	k_{ex} (s^{-1})	p_{ES} (%)	$\Delta\varpi_{GE}$(ppm)
G08 C8	110 ± 9	9.0 ± 0.2	-4.11 ± 0.01	124 ± 10	9.1 ± 0.2	-4.08 ± 0.01
G08 C1'			3.41 ± 0.01			3.38 ± 0.01
G10 C8			-3.99 ± 0.01			-4.03 ± 0.01
G10 C1'			2.40 ± 0.01			2.45 ± 0.01

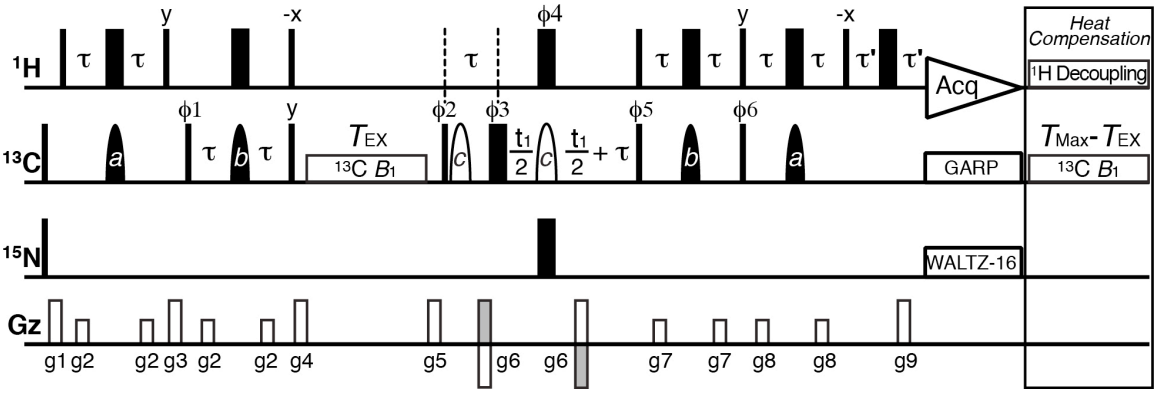

Figure S1. 2D ^{13}C HSQC CEST pulse sequence for measuring ^{13}C-^{1}H splittings in the ground and excited states of nucleic acids. This experiment is essentially the same as previously developed nucleic-acid-optimized 2D ^{13}C HSQC CEST pulse sequence,[1] except there is no ^{1}H decoupling during the relaxation period (T_{EX}) in the present sequence. Narrow (wide) rectangles are hard 90° (180°) pulses, and close (open) shapes are selective on (off) resonance 180° pulses. All pulses are applied along the x-axis unless indicated otherwise and all phases are for Bruker Spectrometers. Shaped pulse *a* selectively inverts carbon magnetization of interest while shaped pulse *b* and *c* selectively refocus and invert carbon magnetization to refocus carbon-carbon scalar couplings. The ^{1}H carrier is kept on water resonance throughout the experiment, while the ^{13}C carrier is kept on-resonance throughout the experiment and is shifted to a desired offset during T_{EX}. Inter-pulse delays are $\tau = 1/4J_{CH}$ and $\tau' = g_9$. The phase cycle used is $\phi_1 = \{x, -x\}$, $\phi_2 = \{y\}$, $\phi_3 = \{2x, 2y, 2(-x), 2(-y)\}$, $\phi_4 = \{4x, 4(-x)\}$, $\phi_5 = \{4x, 4(-x)\}$, $\phi_6 = \{4y, 4(-y)\}$, receiver = $\{x, -x, -x, x, -x, x, x, -x\}$. A minimum of four scans can be used. Gradients with smoothed-square shape (SMSQ10.100) profile are applied with the following strength (G/cm)/duration (ms): g_1 = -33/0.8, g_2 = 4.62/0.6, g_3 = 46.2/0.8, g_4 = 46.2/0.8, g_5 = 46.2/0.8, g_6 = 59.4/0.6, g_7 = 4.62/0.6, g_8 = 4.62/0.6, g_9 = 29.9/0.6. Quadrature detection is achieved using an enhanced sensitivity gradient scheme in which separate data sets are recorded during t_1 period with (ϕ_6, g6) and (ϕ_6 + 180°, -g6), and axial peaks are shifted to the edge of the spectrum by incrementing ϕ_2 and receiver phase by 180° for each t_1 increment. ^{13}C and ^{15}N decoupling during acquisition are achieved using 2.5 kHz GARP and 1.25 kHz WALTZ-16, respectively. To ensure uniform heating, a heat compensation scheme is employed after the acquisition with length of T_{MAX} - T_{EX}, where T_{MAX} is the maximum relaxation delay time, and far off-resonance for both ^{1}H and ^{13}C channels.

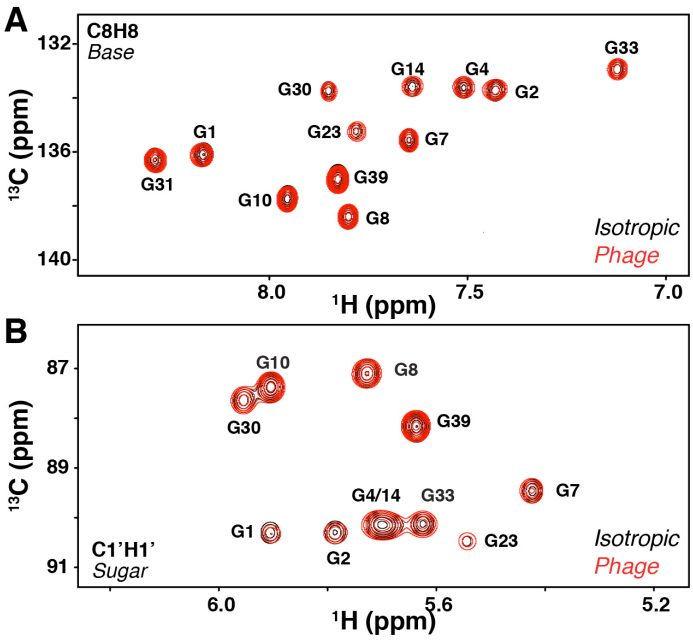

Figure S2. Pf1 phage alignment media does not interfere with the structural integrity of the ligand-free fluoride riboswitch. 2D ^{13}C-^{1}H HSQC base and sugar spectra of the ligand-free *Bacillus cereus* fluoride riboswitch in the isotropic condition (in black) overlaid onto corresponding spectra recorded in the presence of 9.7 mg/ml Pf1 phage alignment media (in red).

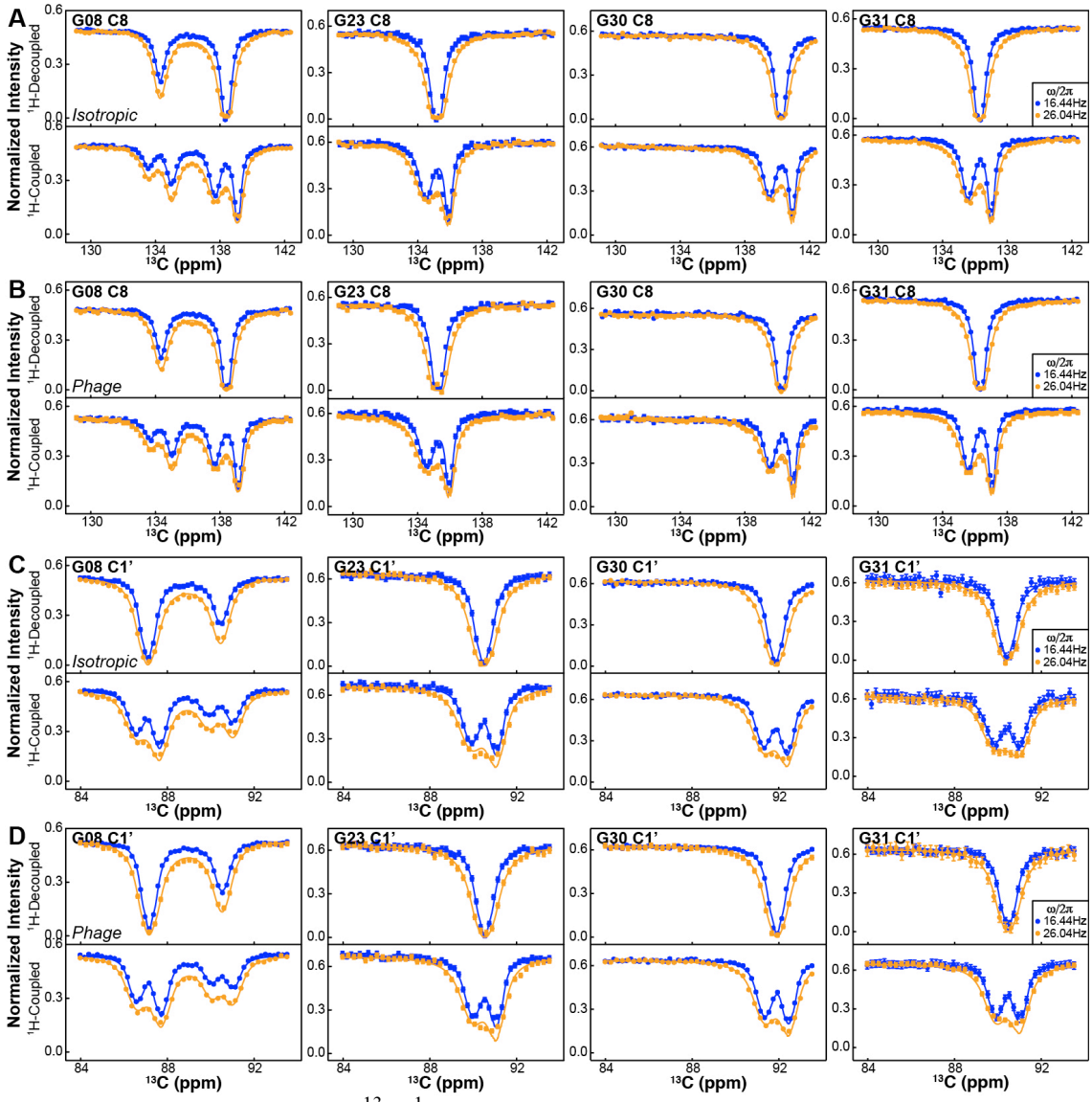

Figure S3. Measurement of ^{13}C-^{1}H splittings of the ground and an "invisible" excited state in the ligand-free *Bacillus cereus* fluoride riboswitch by ^{13}C HSQC CEST experiments. (A-B) Base (C8) ^{13}C HSQC CEST profiles of G8, G23, G30, and G31 measured in the absence (A) and presence (B) of 9.7 mg/ml Pf1 phage alignment media. (C-D) Sugar (C1') ^{13}C HSQC CEST profiles of G8, G23, G30, and G31 measured in the absence (C) and presence (D) of 9.7 mg/ml Pf1 phage alignment media. Solid lines represent best joint-fits of ^{1}H-decouped and ^{1}H-coupled ^{13}C HSQC CEST profiles.

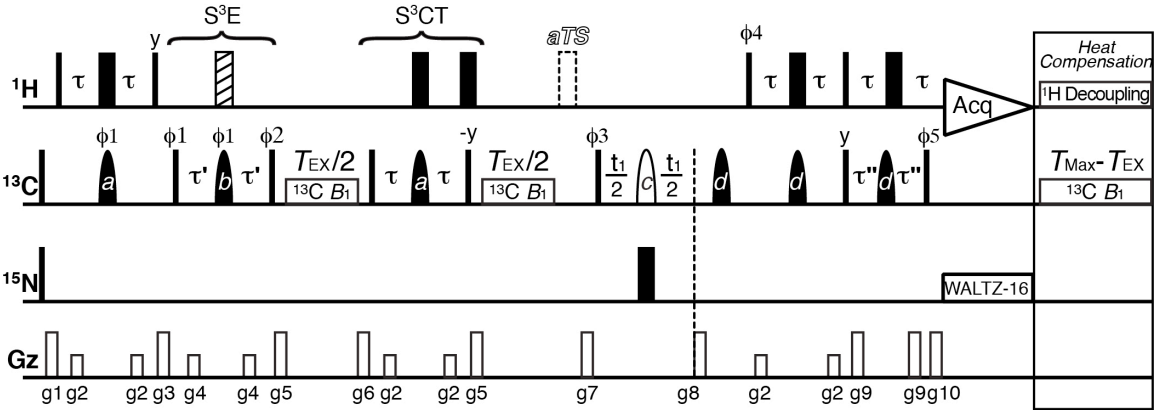

Figure S4. 2D ^{13}C TROSY/anti-TROSY selected (TS/aTS) CEST pulse sequences for characterizing slow conformational exchange and measuring ^{13}C-^{1}H splittings in the ground and excited states of nucleic acids. These nucleic-acid-optimized sequences employ schemes developed in the TS $R_{1\rho}$ RD,[8] CPMG RD RDC,[9] ^{15}N TROSY CEST,[10] and nucleic-acid-optimized TROSY-detected (TD) $R_{1\rho}$ spin relaxation[11] experiments. Narrow (wide) rectangles are hard 90° (180°) pulses, and close (open) shapes are selective on (off) resonance 180^{o} pulses. All pulses are applied along the x-axis unless indicated otherwise and all phases are for Bruker Spectrometers. Shaped pulse *a* selectively inverts carbon magnetization of interest while shaped pulses *b(d)* and *c* selectively refocus and invert carbon magnetization to refocus carbon-carbon scalar couplings. The hatched bar corresponds to a composite ^{1}H 90_{x}^{o}-180_{y}^{o}-90_{x}^{o} pulse. The dashed bar correspond to a ^{1}H 180^{o} pulse present only in the aTS sequence. The ^{1}H carrier is kept on water resonance throughout the experiment, while the ^{13}C carrier is kept on-resonance throughout the experiment and is shifted to a desired offset during T_{EX}. Inter-pulse delays are $\tau = 1/4J_{CH}$, $\tau' = 1/8J_{CH}$, and $\tau'' = \tau - 1/2g10$. The phase cycle used is $\phi_1 = \{x, -x\}$, $\phi_2 = \{4(135^{o})\ 4(315^{o})\}$ for TS and $\{4(45^{o})\ 4(225^{o})\}$ for aTS, $\phi_3 = \{y\ y, -y, -y\}$, $\phi_4 = \{-y\}$, $\phi_5 = \{-x\}$, receiver = $\{x, -x, -x, x, -x, x, x, -x\}$. Gradients with smoothed-square shape (SMSQ10.100) profile are applied with the following strength (G/cm)/duration (ms): g_1 = 33/1.0, g_2 = 3.3/0.25, g_3 = 52.8/1.0, g_4 = 3.3/0.25, g_5 = 26.4/0.5, g_6 = 26.4/0.5, g_7 = 21.8/1.0, g_8 = 46.2/0.6, g_9 = 33/0.15, g_{10} = 46.4/0.15. Quadrature detection is achieved using Rance-Kay echo-antiecho scheme[20,21] in which separate data sets are recorded during t_1 period with (ϕ_4, ϕ_5, g_7) and (ϕ_4+180^{o}, ϕ_5+180^{o}, -g_7),[22] and axial peaks are shifted to the edge of the spectrum by incrementing ϕ_3 and receiver phase by 180^{o} for each t_1 increment. ^{15}N decoupling during acquisition is achieved using 1.25 kHz WALTZ-16. To ensure uniform heating, a heat compensation scheme is employed after the acquisition with length of T_{MAX} - T_{EX}, where T_{MAX} is the maximum relaxation delay time, and far off-resonance for both ^{1}H and ^{13}C channels.

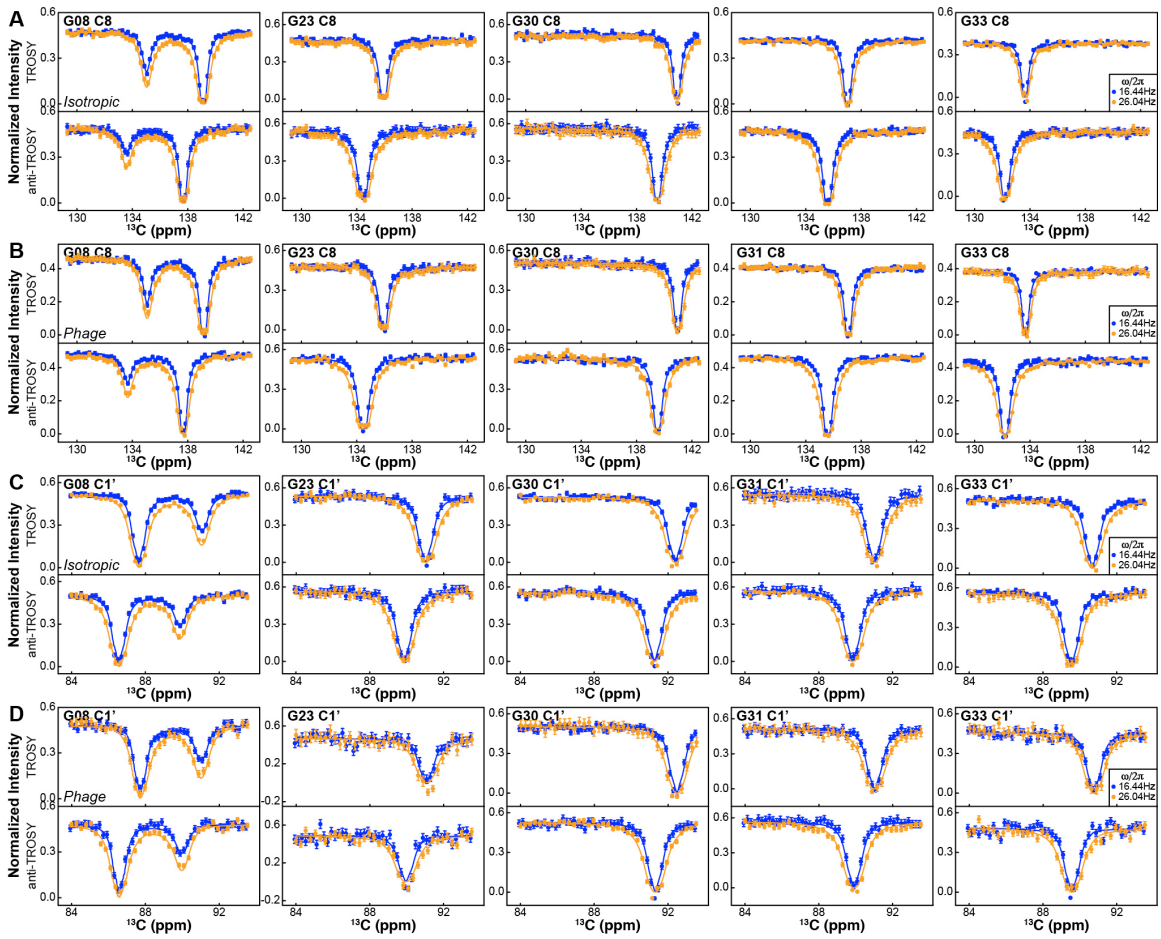

Figure S5. Measurement of ^{13}C-^{1}H splittings of the ground and an "invisible" excited state in the ligand-free *Bacillus cereus* fluoride riboswitch by ^{13}C TROST/anti-TROSY selected (TS/aTS) CEST experiments. (A-B) Base (C8) ^{13}C TS/aTS CEST profiles of G8, G23, G30, G31, and G33 measured in the absence (A) and presence (B) of 9.7 mg/ml Pf1 phage alignment media. (C-D) Sugar (C1') ^{13}C TS/aTS CEST profiles of G8, G23, G30, G31, and G33 measured in the absence (C) and presence (D) of 9.7 mg/ml Pf1 phage alignment media. Solid lines represent best joint-fits of ^{13}C TS/aTS CEST profiles.

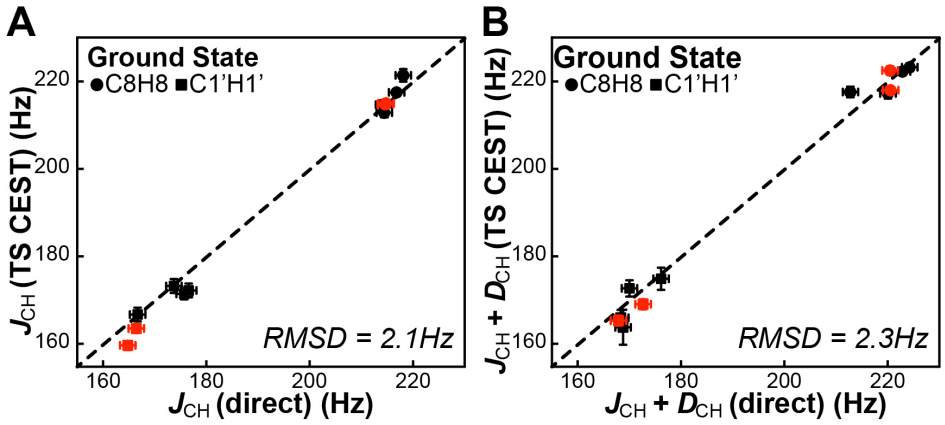

Figure S6. Measurement of ^{13}C-^{1}H splittings by ^{13}C TROST/anti-TROSY selected (TS/aTS) CEST. (A-B) Comparison of ground state (GS) ^{13}C-^{1}H splittings determined from TS/aTS CEST and direct measurements in the absence (A) and presence (B) of 9.7 mg/ml Pf1 phage alignment media. Colored in red are values of G8 and G10.

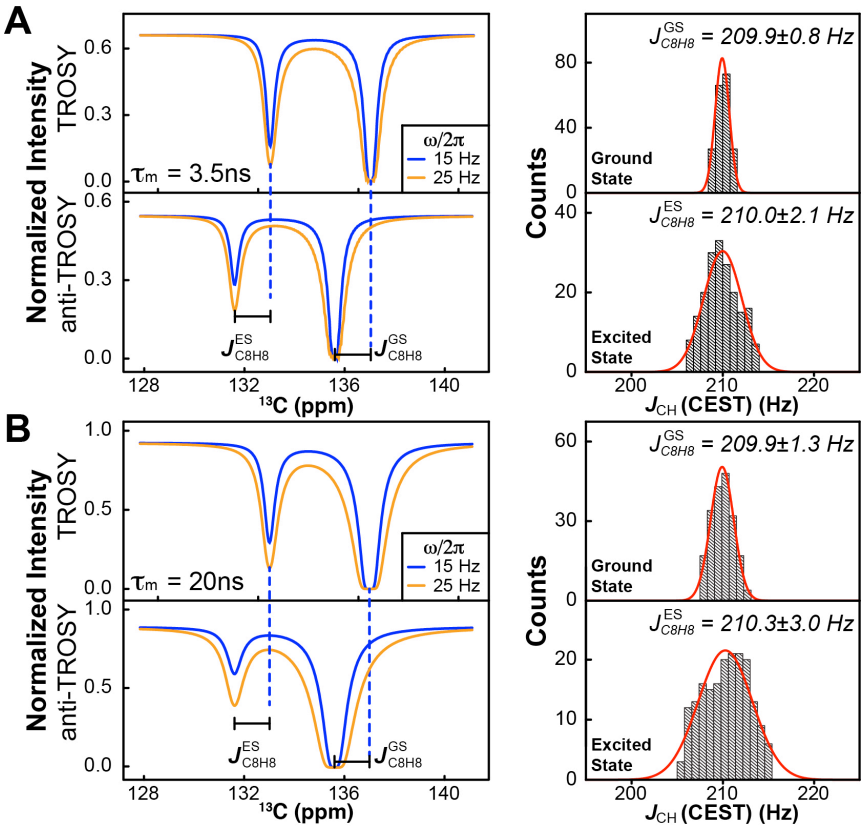

Figure S7. Examining the utility of the TROSY-based CEST experiment in measuring ^{13}C-^{1}H scalar couplings. Two sets of synthetic TROSY and anti-TROSY (TS/aTS) ^{13}C CEST profiles, representing (A) small and (B) large RNAs, were calculated with exchange parameters of k_{ex} = 100 s^{-1}, p_E = 10%, $\Delta\varpi_{GE}$ = 4.0 ppm. ^{13}C-^{1}H scalar couplings ($^{1}J_{CH}$ = 210 Hz) and relaxation parameters of both ground and excited states were assumed to be identical. (A) Numerical simulations of a small RNA were performed using R_1 = 2.58 s^{-1}, R_2 = 20.3 s^{-1}, η_z = 1.20 s^{-1}, η_{xy} = 10.2 s^{-1}, which were calculated using an overall tumbling time (τ_m) of 3.5 ns at ^{1}H Larmor frequency (ω_H) of 600.133 MHz. (B) Numerical simulations of a large RNA were performed using R_1 = 0.49 s^{-1}, R_2 = 108.2 s^{-1}, η_z = 0.23 s^{-1}, η_{xy} = 55.0 s^{-1}, which were calculated using τ_m = 20 ns and ω_H = 600.133 MHz. Given almost identical calculated values between R_{1HC} (R_{2HC}) and R_1 (R_2), R_{1HC} (R_{2HC}) were assumed to be the same as R_1 (R_2) in the simulations. CEST profiles at two ^{13}C B_1 fields ($\omega/2\pi$ = 15 and 25 Hz) were generated using T_{EX} of 0.3s and 0.16s for TS and aTS profiles, respectively. A Gaussian error of 3%, which corresponds to the high end of our observed experimental errors, was then randomly added to each synthetic data point to generate a total of 200 randomly perturbed data sets. These data sets were fit individually to extract $^{1}J_{CH}$ values of both the ground and excited states. Distributions of the extracted $^{1}J_{CH}$ values are shown in the right panels with Gaussian lines in red. The $^{1}J_{CH}$ values shown in the figures are mean ± standard deviation for the 200 best-fit values. As can be seen, despite much broader TS/aTS intensity dips at τ_m = 20ns, a typical tumbling time for a ~25kDa RNA or a ~50kDa protein, the $^{1}J_{CH}$ values of both the ground and excited states can be reliably obtained as evidenced by relatively small standard deviations, strongly supporting the applicability of the TS/aTS CEST approach in measuring ^{13}C-^{1}H scalar couplings over a wide range of molecular weights.

Supporting Information References

(1) Zhao, B.; Hansen, A. L.; Zhang, Q. *J. Am. Chem. Soc.* **2014**, *136*, 20.

(2) Meissner, A.; Sorensen, O. W. *J. Magn. Reson.* **1999**, *139*, 439.

(3) Bailor, M. H.; Musselman, C.; Hansen, A. L.; Gulati, K.; Patel, D. J.; Al-Hashimi, H. M. *Nat. Protoc.* **2007**, *2*, 1536.

(4) Delaglio, F.; Grzesiek, S.; Vuister, G. W.; Zhu, G.; Pfeifer, J.; Bax, A. *J. Biomol. NMR* **1995**, *6*, 277.

(5) Johnson, B. A.; Blevins, R. A. *J. Biomol. NMR* **1994**, *4*, 603.

(6) Guenneugues, M.; Berthault, P.; Desvaux, H. *J. Magn. Reson.* **1999**, *136*, 118.

(7) Pervushin, K.; Riek, R.; Wider, G.; Wuthrich, K. *Proc. Natl. Acad. Sci. U.S.A.* **1997**, *94*, 12366.

(8) Igumenova, T. I.; Palmer, A. G., 3rd *J. Am. Chem. Soc.* **2006**, *128*, 8110.

(9) Vallurupalli, P.; Hansen, D. F.; Stollar, E.; Meirovitch, E.; Kay, L. E. *Proc. Natl. Acad. Sci. U.S.A.* **2007**, *104*, 18473.

(10) Long, D.; Bouvignies, G.; Kay, L. E. *Proc. Natl. Acad. Sci. U.S.A.* **2014**, *111*, 8820.

(11) Hansen, A. L.; Al-Hashimi, H. M. *J. Am. Chem. Soc.* **2007**, *129*, 16072.

(12) Meissner, A.; Duus, J. O.; Sorensen, O. W. *J. Magn. Reson.* **1997**, *128*, 92.

(13) Sorensen, M. D.; Meissner, A.; Sorensen, O. W. *J. Biomol. NMR* **1997**, *10*, 181.

(14) Mcconnell, H. M. *J. Chem. Phys.* **1958**, *28*, 430.

(15) Allard, P.; Helgstrand, M.; Hard, T. *J. Magn. Reson.* **1998**, *134*, 7.

(16) Helgstrand, M.; Hard, T.; Allard, P. *J. Biomol. NMR* **2000**, *18*, 49.

(17) Hansen, A. L.; Kay, L. E. *Proc. Natl. Acad. Sci. U.S.A.* **2014**, *111*, E1705.

(18) Vallurupalli, P.; Kay, L. E. *Angew. Chem. Int. Ed. Engl.* **2013**, *52*, 4156.

(19) Dethoff, E. A.; Petzold, K.; Chugh, J.; Casiano-Negroni, A.; Al-Hashimi, H. M. *Nature* **2012**, *491*, 724.

(20) Kay, L. E.; Keifer, P.; Saarinen, T. *J. Am. Chem. Soc.* **1992**, *114*, 10663.

(21) Palmer, A. G.; Cavanagh, J.; Wright, P. E.; Rance, M. *J. Magn. Reson.* **1991**, *93*, 151.

(22) Weigelt, J. *J. Am. Chem. Soc.* **1998**, *120*, 10778.